

A Graph-Augmented knowledge Distillation based Dual-Stream Vision Transformer with Region-Aware Attention for Gastrointestinal Disease Classification with Explainable AI

Md. Assaduzzaman^{1*}, Nushrat Jahan Oyshi¹, Eram Mahamud¹

¹ Department of Computer Science and Engineering

Daffodil International University

Dhaka 1207, Bangladesh

Abstract

The accurate classification of gastrointestinal diseases from endoscopic and histopathological imagery remains a significant challenge in medical diagnostics, mainly due to the vast data volume and subtle variation in inter-class visuals. This study presents a hybrid dual-stream deep learning framework built on teacher-student knowledge distillation, where a high-capacity teacher model integrates the global contextual reasoning of a Swin Transformer with the local fine-grained feature extraction of a Vision Transformer. The student network was implemented as a compact Tiny-ViT structure that inherits the teacher's semantic and morphological knowledge via soft-label distillation, achieving a balance between efficiency and diagnostic accuracy. Two carefully curated Wireless Capsule Endoscopy datasets, encompassing major GI disease classes, were employed to ensure balanced representation and prevent inter-sample bias. The proposed framework achieved remarkable performance with accuracies of 0.9978 and 0.9928 on Dataset 1 and Dataset 2 respectively, and an average AUC of 1.0000, signifying near-perfect discriminative capability. Interpretability analyses using Grad-CAM, LIME, and Score-CAM confirmed that the model's predictions were grounded in clinically significant tissue regions and pathologically relevant morphological cues, validating the framework's transparency and reliability. The Tiny-ViT demonstrated diagnostic performance with reduced computational complexity comparable to its transformer-based teacher while delivering faster inference, making it suitable for resource-constrained clinical environments. Overall, the proposed framework provides a robust, interpretable, and scalable solution for AI-assisted GI disease diagnosis, paving the way toward future intelligent endoscopic screening that is compatible with clinical practicality.

Keywords: Gastrointestinal disease classification; Wireless Capsule Endoscopy (WCE); Knowledge Distillation; Swin Transformer; Vision Transformer; Deep Learning; Explainable Artificial Intelligence (XAI); Grad-CAM; LIME; Score-CAM; Medical Image Analysis; Computer-Aided Diagnosis (CAD)

1. Introduction

Gastrointestinal (GI) diseases such as colorectal polyps, esophagitis, and ulcerative colitis are among the most common and potentially serious conditions affecting the human digestive system. If left undiagnosed, these diseases can lead to complications including chronic pain, malnutrition, and in some cases, colorectal cancer, one of the leading causes of cancer-related deaths globally. Early detection and timely treatment are essential for improving patient outcomes and reducing the global disease burden. One of the most effective diagnostic tools for identifying abnormalities in the GI tract is Wireless Capsule Endoscopy (WCE). WCE involves swallowing a small capsule equipped with a camera that captures thousands of high-resolution images as it passes through the digestive tract. While this technology has significantly improved diagnostic coverage, the sheer volume of images produced during a single session, often over 50,000 frames, creates a significant bottleneck for clinicians. Manually reviewing these images is time-consuming, labour-intensive, and prone to human error or oversight, particularly when abnormalities are subtle or infrequent [1].

In recent years, deep learning techniques, especially Convolutional Neural Networks (CNNs), have shown great potential in automating medical image classification tasks [2]. Several studies have applied CNNs to endoscopy images and demonstrated promising results in detecting specific GI disorders. However, these methods are often

limited by the quality and structure of the datasets used. Many public WCE datasets are either too small, unbalanced in class distribution, or contain overlapping samples across training and test splits, leading to biased evaluation and overfitting. In real clinical settings, such shortcomings can undermine the reliability and generalizability of AI models [3,4].

To address these limitations, we use the WCE Curated Colon Disease Dataset, a well-structured and class-balanced dataset created by aggregating and refining samples from established public datasets, including KVASIR and ETIS-Larib-Polyp [5]. This curated dataset contains four clearly defined disease categories: normal mucosa, ulcerative colitis, polyps, and esophagitis with equal representation, ensuring more stable model training and fair evaluation. The dataset has been pre-processed and carefully split to avoid data leakage between training and testing sets, which is critical for maintaining the integrity of model performance metrics [6].

Building upon this dataset, we propose a robust deep learning framework for the automated classification of GI tract conditions from endoscopy images. Our model is designed to extract and combine both local and global image features using multi-scale feature extraction layers and attention mechanisms. In addition, we apply advanced preprocessing techniques, including image enhancement and data augmentation, to improve model robustness and generalisation to unseen samples. The entire pipeline is optimised to minimise overfitting while ensuring high classification accuracy across all four disease categories.

The main contributions of this paper are as follows:

- A dual-stream Transformer teacher architecture is introduced, combining Swin Transformer for global contextual modeling with ViT-16 for detailed morphological feature extraction.
- A compact Tiny-ViT student model is developed using soft-label knowledge distillation, enabling efficient inference with minimal performance loss.
- A region-aware attention mechanism and multi-scale feature fusion strategy are incorporated to enhance focus on clinically salient gastrointestinal regions.
- Extensive evaluation on wireless capsule endoscopy and colorectal histopathology datasets demonstrates strong cross-modal generalization with accuracies exceeding 99%.
- Multiple XAI techniques, including Grad-CAM, Grad-CAM++, Score-CAM, and LIME, are employed to verify that classification decisions correspond to anatomically and pathologically meaningful regions.

The findings of this work are expected to support gastroenterologists by providing a fast and reliable second-opinion system. Ultimately, our goal is to reduce diagnostic delays and improve early detection of potentially life-threatening GI conditions by integrating AI-driven solutions into clinical workflows.

2. Related Works

Artificial intelligence is now central to computer-aided diagnosis of gastrointestinal and colorectal cancer. Recent studies have applied deep learning to histopathology and endoscopy images, prognosis, risk assessment, and biomarker discovery. This section summarizes key research areas and shows how our work relates to them.

Le et al. [7] showed that using CNNs for classifying CRC histopathology can significantly identify subtle glandular variations and structural distortions in tissue slides, especially boosting diagnostic accuracy for challenging tumor cases. Ömeroğlu et al. [8] improved representation learning using supervised contrastive training, which made features easier to separate. However, their method needed a lot of GPU resources and careful tuning, showing the effort required. Fadafan and Rezaee et al. [9] used hybrid CNN-transformer modules to improve consistency in recognizing different CRC tissue types. However, their model requires several GPUs and takes more time to run. El Amine et al. [10] used semi-supervised ViT models with GAN-based normalization to improve domain adaptation, but the training process was complex and hard to use in clinics. Ke

et al. [11] developed networks for analyzing CRC at different magnifications, but these faced problems with patch redundancy and sensitivity to changes in magnification.

Parallelly, Mirza et al. [12] introduced a dual-depth CNN fusion model for classifying WCE diseases. This model improved detection of lesion boundaries but still lacked enough regional interpretability. Bordbar et al. [13] used a 3D convolutional structure to track lesion progression in capsule sequences, but this approach needed much more memory. To improve the explainability, Shukla and Jayaraman et al. [14] applied Grad-CAM and LIME, but the visual reasoning was still qualitative and not suitable for diagnostic certification. Attallah et al. [15] developed a multiscale attention-based network that improved detection accuracy for gastrointestinal abnormalities, but it did not work as well across different institutions. Tan et al. [16] created EndoOOD to improve out-of-distribution modeling in capsule imaging, making diagnosis more reliable but still lacking detailed interpretation of lesion contexts.

Recent studies have used advanced deep learning for CRC classification and GI analysis. Le et al. [17] applied deep learning to category-level CRC histopathology, showing reliable tissue discrimination. Chung et al. [18] built a framework for automatic GI organ classification in capsule endoscopy whereas Sharma et al. [19] developed a model to diagnose GI diseases from endoscopy images proposing better accuracy. Various framework-based solutions have been investigated for generalization of such image classification. Rahaman et al. [20] created HistopathAI to generalize histopathology image classification across datasets. Khan et al. [21] proposed a lightweight deep learning method for identifying GI diseases from WCE images, focusing on efficiency. They have also explored fine-tuning and optimization to improve model performance. AlGhafri and Lim [22] studied fine-tuning for better feature adaptation in CRC classification.

Multiple approaches based on Neural Network architecture were proposed for gastrointestinal disease identification and some of them go beyond imaging approaches. Rajkumar et al. [23] introduced GastroNet, a CNN system for detecting GI abnormalities in WCE images. Elforaici et al. [24] presented a semi-supervised ViT-based framework for predicting survival in colorectal liver metastases. Ke et al. [25] created an ensemble deep learning model with transfer learning for multi-class CRC histopathology. Gondal and Farooqi [26] studied non-coding RNA mechanisms in CRC using single-cell transcriptomics. Some studies have focused on prognosis and survival prediction. Nguyen et al. [27] used machine learning feature extraction for CRC classification in biomedical engineering. Huang et al. [28] built a deep learning system to assess risk in stage II colorectal cancer using CT and pathology data. Tafavvoghi et al. [29] proposed a deep learning model to predict mismatch repair deficiency from a single slide. Westwood et al. [30] showed that tumor cell and lymphocyte density, measured by deep learning, can help predict outcomes.

Alsubai [31] combined local binary patterns, transfer learning, and explainable AI to detect lung and colon cancer which caught a lot of attention. His research looked at early screening and large-scale validation. Chang et al. [32] used AI-enhanced feature engineering to study nanoscale chromatin changes for early CRC screening. Yuan et al. [33] built and validated a transfer learning-based CRC diagnostic system in a large study. Alotaibi et al. [34] proposed an ensemble deep learning model for early detection of lung and colon cancer from histopathology images. Jiang et al. [35] developed an end-to-end deep learning model for CRC prognosis using data from multiple centers. Foersch et al. [36] used multistain deep learning to predict prognosis and therapy response in CRC.

Datasets and surveys have been important for GI disease research. Desai et al. [37] studied few-shot learning for CRC histopathology image classification. Sharma and Lamba [38] reviewed deep learning models for understanding WCE images. Chen et al. [41] developed an AI-based CNN system for automated capsule endoscopy recognition. Several review studies have discussed current challenges and limitations. El-Gammal et al. [42] reviewed AI models for capsule endoscopy and pointed out issues with robustness and clinical use. Temesgen et al. [43] suggested a transformer-based method for real-time object detection in WCE videos.

Kar and Rowlands [44] looked at how deep learning systems can be used for CRC diagnosis with histopathology images. Frasca et al. [45] reviewed deep learning frameworks for CRC image processing.

George et al. [46] discussed the current state and future of AI in capsule endoscopy. Recent studies have focused on explainability, robustness, and dataset quality. Bhatty et al. [47] used deep learning for colon cancer classification with histopathology images. Mahi [48] reviewed deep learning models for WCE image analysis. Chlorogiannis et al. [49] assessed if deep learning-based CRC diagnosis systems are ready for clinical use. Alfa et al. [50] proposed an accurate CAD system for GI abnormalities in capsule endoscopy. Mahamud et al. [51] showed explainable AI models for lung disease classification using transfer learning. Mahamud et al. [52] studied explainable ensemble learning for Alzheimer's detection. Despite these achievements, several limitations persist in existing research. Many models rely on single-modality datasets and lack cross-centre generalisation. Others focus solely on image-level classification, neglecting the temporal and contextual relationships in WCE video streams. Additionally, interpretability remains an open challenge, as most frameworks provide only coarse attention maps without anatomical reasoning. To address these issues, the present Study introduces a dual-stream hybrid framework that fuses global (Swin Transformer Small) and local (ViT-16 Small) feature representations within a teacher–student knowledge-distillation paradigm. The proposed Tiny-ViT student model inherits both semantic context and morphological precision from the transformer teacher, achieving high accuracy and interpretability while remaining computationally efficient for real-time clinical application.

Table 1. Critical Analysis of Related Works on AI-Based Colorectal Cancer (CRC) Detection

Study (Ref), Year	Focus Area	Model / Technique	Key Limitations
Le et al. [7], 2025	CRC tissue classification	CNN-based hierarchical classifier	Limited interpretability; lacks cross-dataset validation
Ömeroğlu et al. [8], 2024	CRC histopathology	Supervised contrastive + ResNet	High training cost; small-scale generalization
Fadafen & Rezaee [9], 2023	Multi-tissue CRC	Hybrid CNN + Transformer (HCT-Net)	Requires multiple GPUs; complex architecture
El Amine et al. [10], 2023	Semi-supervised diagnosis	ViT + GAN-based normalization	Complex pipeline; challenges in clinical deployment
Ke et al. [11], 2025	Multi-magnification CRC	Cross-resolution CNN ensemble	Redundancy at patch level; overfitting risks
Mirza et al. [12], 2025	GI disease (WCE)	Dual-depth CNN fusion	Lacks regional interpretability; small dataset
Bordbar et al. [13], 2023	WCE video analysis	3D Deep CNN (ResNet-50 3D)	High memory usage due to 3D convolutions
Shukla & Jayaraman [14], 2025	Explainable AI in WCE	CNN + Grad-CAM / LIME	Visual reasoning is qualitative, not diagnostic-certified
Attallah et al. [15], 2025	GI abnormalities	Multiscale Attention Network (EndoNet)	Generalization across institutions is constrained
Tan et al. [16], 2024	OOD detection (WCE)	EndoOOD (Uncertainty-aware)	Focuses on out-of-distribution; lacks hierarchical context
Le et al. [17], 2025	Category detection	Deep learning classification	Focused on specific categories; limited structural analysis
Chung et al. [18], 2023	GI Organ Classification	Deep learning framework	Limited to organ classification, not specific pathology

Sharma et al. [19], 2023	GI Disease Prediction	Deep learning prediction model	Accuracy varies across different disease classes
Rahaman et al. [20], 2025	General Histopathology	HistopathAI Framework	Computationally intensive for large-scale deployment
Khan et al. [21], 2024	Lightweight GI ID	Lightweight Deep Learning	Trade-off between model size and complex feature capture
AlGhafri & Lim [22], 2025	Fine-tuning CRC	Fine-tuned CNN models	Requires precise hyperparameter tuning per dataset
Rajkumar et al. [23], 2024	GI Abnormalities	GastroNet (CNN-based)	Specific to certain abnormality types
Elforaici et al. [24], 2025	Survival Prediction	Semi-supervised ViT + KD	High complexity; requires survival data labels
Ke et al. [25], 2025	Multi-class CRC	Transfer Learning + Ensemble	Ensemble adds latency; heavy computational load
Gondal & Farooqi [26], 2025	Non-coding RNA	Single-cell transcriptomics	Bioinformatics focus; less direct clinical imaging application
Nguyen et al. [27], 2025	Feature Extraction	Machine Learning (Feature-based)	Less robust than end-to-end DL for complex textures
Huang et al. [28], 2025	Risk Stratification	CT + Pathological Markers DL	Multimodal data requirement limits accessibility
Tafavvoghi et al. [29], 2025	MMR Deficiency	Single-slide DL Model	Prediction relies heavily on slide quality
Westwood et al. [30], 2025	Prognostic Biomarker	DL for Cell Density (TILs)	Quantitative focus; requires precise segmentation
Alsubai [31], 2024	Lung & Colon Ca.	LBP + Transfer Learning + XAI	Hand-crafted features (LBP) may miss abstract patterns
Chang et al. [32], 2024	Early Screening	AI + Nanoscale Chromatin Eng.	Requires specialized imaging/engineering setup
Yuan et al. [33], 2024	External Validation	Transfer Learning System	Performance drops slightly on non-emulated external data
Alotaibi et al. [34], 2024	Early Detection	Ensemble Deep Learning	Ensemble complexity affects real-time inference speed
Jiang et al. [35], 2024	Prognostication	End-to-end DL Model	Black-box nature limits clinical trust in prognosis
Foersch et al. [36], 2023	Therapy Response	Multistain Deep Learning	Dependency on multiple stain availability
Desai et al. [37], 2024	Few-shot Learning	Few-shot Histopathology	Lower accuracy compared to fully supervised methods
Sharma & Lamba [38], 2025	Model Analysis	Review / Analysis	Theoretical analysis; no proposed novel architecture

Chen et al. [41], 2024	WCE Recognition	CNN-based System	Standard CNN architecture; limited novelty
El-Gammal et al. [42], 2025	Survey (WCE)	AI Models Survey	Highlights robustness issues; no new model proposed
Temesgen et al. [43], 2025	Real-time Detection	Transformer-based (Object Det.)	High computational cost for real-time video
Kar & Rowlands [44], 2024	Clinical Assessment	DL System Assessment	Focuses on applicability rather than algorithm design
Frasca et al. [45], 2025	Framework Review	DL Frameworks Review	Review of existing frameworks; no new implementation
George et al. [46], 2024	Future Expectations	AI in Capsule Endoscopy	Theoretical discussion on future trends
Bhatty et al. [47], 2023	Colon Cancer Class.	Deep Learning Techniques	Standard DL application; limited innovation
Mahi [48], 2023	WCE Review	DL Models Review	General overview; lacks in-depth technical critique
Chlorogiannis et al. [49], 2023	Clinical Readiness	Readiness Evaluation	Identifies gap between research accuracy and clinical use
Alfa et al. [50], 2024	CAD System	Accurate DL System	Accuracy focus; less emphasis on explainability
Mahamud et al. [51], 2024	Lung Disease (XAI)	Transfer Learning + XAI	Domain specific (Lung); transferability to GI verified?
Mahamud et al. [52], 2025	Alzheimer's (XAI)	Ensemble Learning + XAI	Domain specific (Brain); highlights XAI utility

Table 1. Critical Analysis of Related Works on AI-Based Colorectal Cancer (CRC) Detection

Together, these studies underline the growing importance of AI in colorectal cancer diagnosis. They show how combining image analysis, genetic data, and clinical features can lead to more accurate, faster, and explainable outcomes. Inspired by these developments, our Study builds on transformer-based models to enhance the reliability and interpretability of CRC diagnosis from histopathological images.

3. Methodology

3.1. Overview

The proposed framework introduces a dual-encoder knowledge distillation paradigm for the automated classification of gastrointestinal (GI) diseases from Wireless Capsule Endoscopy (WCE) images. The architecture employs a teacher–student learning strategy, where the teacher network integrates two complementary vision transformers, Swin Transformer Small (patch4-window7-224) as the global encoder and ViT-Small (patch16-224) as the local encoder. This combination enables the extraction of both macro-level contextual features and micro-level texture representations, essential for differentiating subtle pathological variations in endoscopic imagery. The Swin Transformer captures hierarchical and spatial dependencies across vast receptive fields, while the ViT16 component focuses on localised morphological cues such as glandular structures and mucosal irregularities. The student network, implemented using Tiny-ViT (tiny_vit_5m_224), serves as a lightweight, computationally efficient alternative that can reproduce the teacher's diagnostic capability under constrained resources. Through knowledge distillation, the student model assimilates both the

explicit supervision from ground-truth labels and the implicit knowledge contained in the teacher’s soft probability distributions, thereby inheriting its discriminative and interpretive strengths while maintaining rapid inference. The overall methodological pipeline, illustrated schematically in Figure 1, encompasses dataset curation, image preprocessing and augmentation, dual-stream architectural design, knowledge transfer via distillation, and comprehensive performance evaluation across multiple metrics and interpretability frameworks. This design ensures a robust, interpretable, and scalable solution for endoscopic disease classification suitable for real-time clinical decision support.

3.2. Dataset Description

3.2.1 Dataset 1

Dataset 1 integrates endoscopic images from two publicly available, clinically curated repositories: the KVASIR dataset [39]. Images were captured using Wireless Capsule Endoscopy (WCE) and released after standardised preprocessing and clear source separation to minimise the risk of patient-level data leakage across splits. Following the Kaggle distribution used in prior work (e.g., Montalbo, 2022), we retained the original folder structure and split strategy and applied only standardisation steps necessary for model ingestion (e.g., resizing to the network input size and per-channel normalisation). The curated set targets four diagnostic categories aligned with common WCE findings: normal mucosa, ulcerative colitis, colorectal polyps, and esophagitis. Labels are inherited from the source repositories and mapped to consistent class identifiers used throughout this Study.

Dataset distribution

The Kaggle release contains 6,000 WCE images organised into train/, val/, and test/ partitions and four class folders per split (0_normal, 1_ulcerative_colitis, 2_polyps, 3_esophagitis). The test partition is explicitly balanced with 200 images per class (total 800 test images). The train/ and val/ partitions follow the same four-class structure and are used as released; class balance is preserved per split for fair evaluation. Table 1 reports the composition of the test split (the portion with verified per-class counts), which we use for final model assessment. Counts for training and validation are taken from the released split and are described alongside implementation details in Section 4 (*Experiments*). Table 2 shows the composition of dataset 1 composition.

Table 2. Dataset 1 (Kaggle WCE Curated) — test split composition

Dataset 1			Dataset 2
Class Label	Pathology Type	Test	Class Label
0_normal	Normal mucosa	200	Tumor
1_ulcerative_colitis	Ulcerative colitis	200	Stroma
2_polyps	Colorectal polyps	200	Other
3_esophagitis	Esophagitis	200	

3.2.2 Dataset 2

Dataset 2 comprises histopathological image patches derived from hematoxylin and eosin (H&E) stained tissue samples of colorectal cancer, collected from 17 patients in the Central Finland Healthcare District. The dataset is publicly available via Mendeley [40]. The dataset contains 2,770 image patches of 224×224 pixels at 0.5 μm per pixel, distributed into three tissue classes: tumour, stroma, and other (including debris, lymphocytes, mucus, normal epithelium, and smooth muscle). Labels were acquired directly from pathologist annotations, which are mapped to consistent class identifiers used throughout the dataset. Table 3 shows the patch distribution per class.

Table 3. Dataset 2 (Mendeley Colorectal Histopathology Patches) — Class Distribution

Class	Number of Patches
Tumor	1,004
Stroma	1,001
Other	765

Total	2,770
-------	-------

Dataset distribution

Depending on the experimental needs, the train/validation/test were distributed, maintaining a 75:15:15 ratio. The dataset is intended for tasks such as external testing of deep learning models for tissue classification and segmentation, as well as for digital pathology studies. The training, validation, and test partitions are balanced across all categories. The distribution is shown in Table 4.

Table 4. Dataset-2 composition and distribution

Class Label	Pathology Type	Train	Validation	Test
0 tumor	Tumor	754	125	125
1 stroma	Stroma	751	125	125
2 other	Other	575	95	95
Total	—	2,080	345	345

3.3. Preprocessing and Augmentation

To standardise the input format across samples and facilitate compatibility with pretrained architectures, all images were resized to 24×224 pixels. Pixel intensities were normalized on a per-channel basis using the mean ($\mu = [0.485, 0.456, 0.406]$) and standard deviation ($\sigma = [0.229, 0.224, 0.225]$) statistics derived from the ImageNet dataset, thereby aligning the dataset's pixel distribution with that of the pretraining domain. For the training subset, a carefully constrained augmentation pipeline was applied generalization while preserving the integrity of pathological features. This included random horizontal flipping to simulate natural variations in capsule orientation, small in-plane rotations ± 10 degrees to reflect realistic endoscopic motion, and mild affine transformations to mimic viewpoint and positional changes. These transformations aimed to expand the representational diversity of the training data without introducing artefacts that could compromise clinical interpretability. The validation and test subsets were strictly limited to resizing and normalisation to maintain a consistent, unbiased evaluation protocol.

3.4. Model Architectures

The overall workflow of the proposed framework is illustrated in Figures 1 and 2, which summarise the end-to-end architecture, including data flow, dual-encoder teacher network, knowledge distillation pipeline, and the lightweight Tiny-ViT student model.

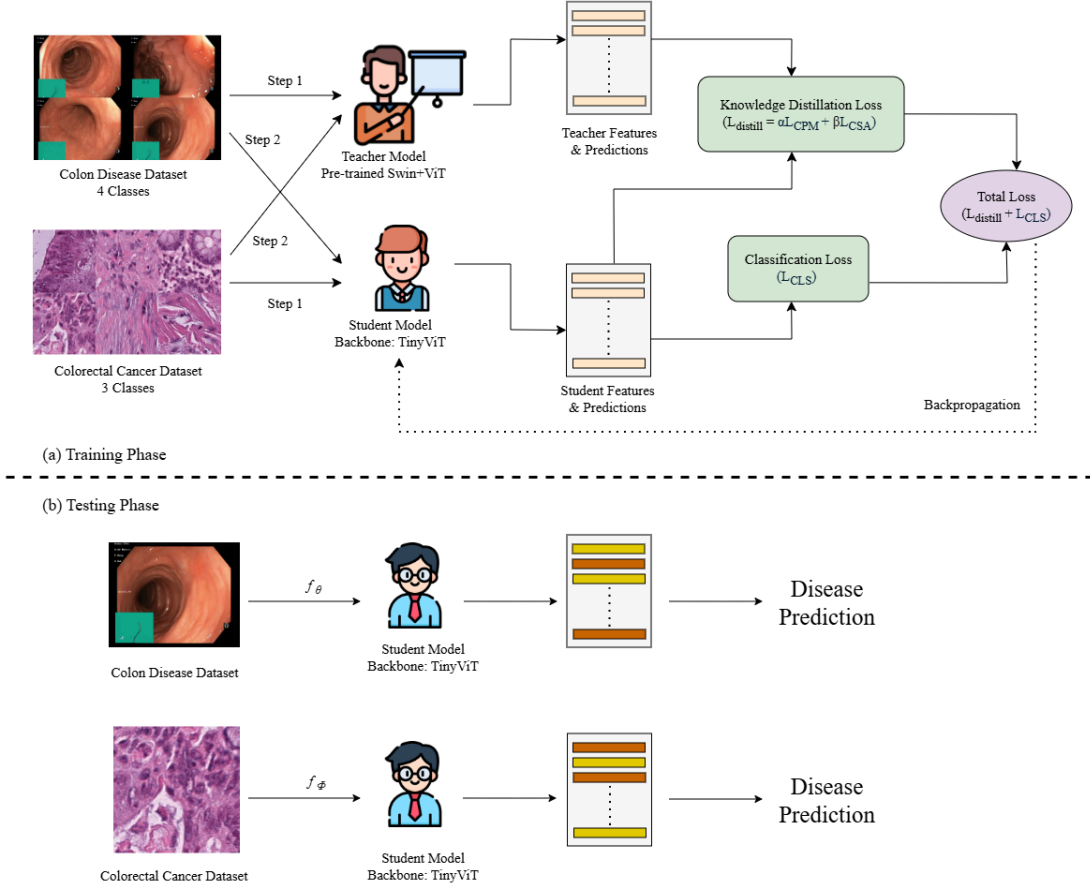


Fig 1. Training and testing phases of the proposed teacher–student knowledge distillation framework.

The proposed framework adopts a teacher–student architecture that integrates a dual-encoder Transformer teacher with a lightweight Tiny-ViT student, designed to achieve both high diagnostic accuracy and computational efficiency in gastrointestinal (GI) disease classification from Wireless Capsule Endoscopy (WCE) imagery. The teacher network incorporates two complementary encoders: a Swin Transformer (Small, patch4-window7-224) serving as the global encoder, and a Vision Transformer (ViT-Small, patch16-224) acting as the local encoder. The Swin Transformer employs a shifted-window self-attention mechanism that hierarchically models long-range dependencies across spatial regions with linear computational complexity relative to image size. This enables the network to capture large-scale contextual relationships such as mucosal patterns and diffuse inflammation. In contrast, the ViT16 module focuses on fine-grained local textures and micro-structural cues, including glandular boundaries, epithelial distortions, and lesion morphology. Features extracted from both encoders are fused using an attention-guided feature aggregation module, which adaptively balances global and local representations. The dual-encoder design thus integrates macroscopic contextual awareness with microscopic precision, providing a comprehensive representation of GI pathology. Both encoders are initialised with ImageNet-1K weights, and early layers are partially frozen to preserve low-level feature generalisation while deeper layers are fine-tuned for domain-specific adaptation. The student model is implemented as Tiny-ViT (tiny_vit_5m_224), a compact Vision Transformer containing approximately 5 million parameters. It retains the essential self-attention structure of standard ViTs while employing depth-reduced transformer blocks and efficient patch embeddings to achieve low latency and reduced memory consumption. During the distillation process, the Tiny-ViT student learns from both hard labels and soft targets generated by the dual-encoder teacher, effectively inheriting its decision boundaries and inter-class relationships. The final classification head outputs four softmax-activated probabilities corresponding to the diagnostic categories: normal mucosa, ulcerative colitis, polyps, and esophagitis. This hybrid configuration ensures that the teacher network provides rich, hierarchical supervision. At the same time, the student model delivers lightweight, real-time inference, a crucial balance for practical deployment in clinical endoscopy workflows.

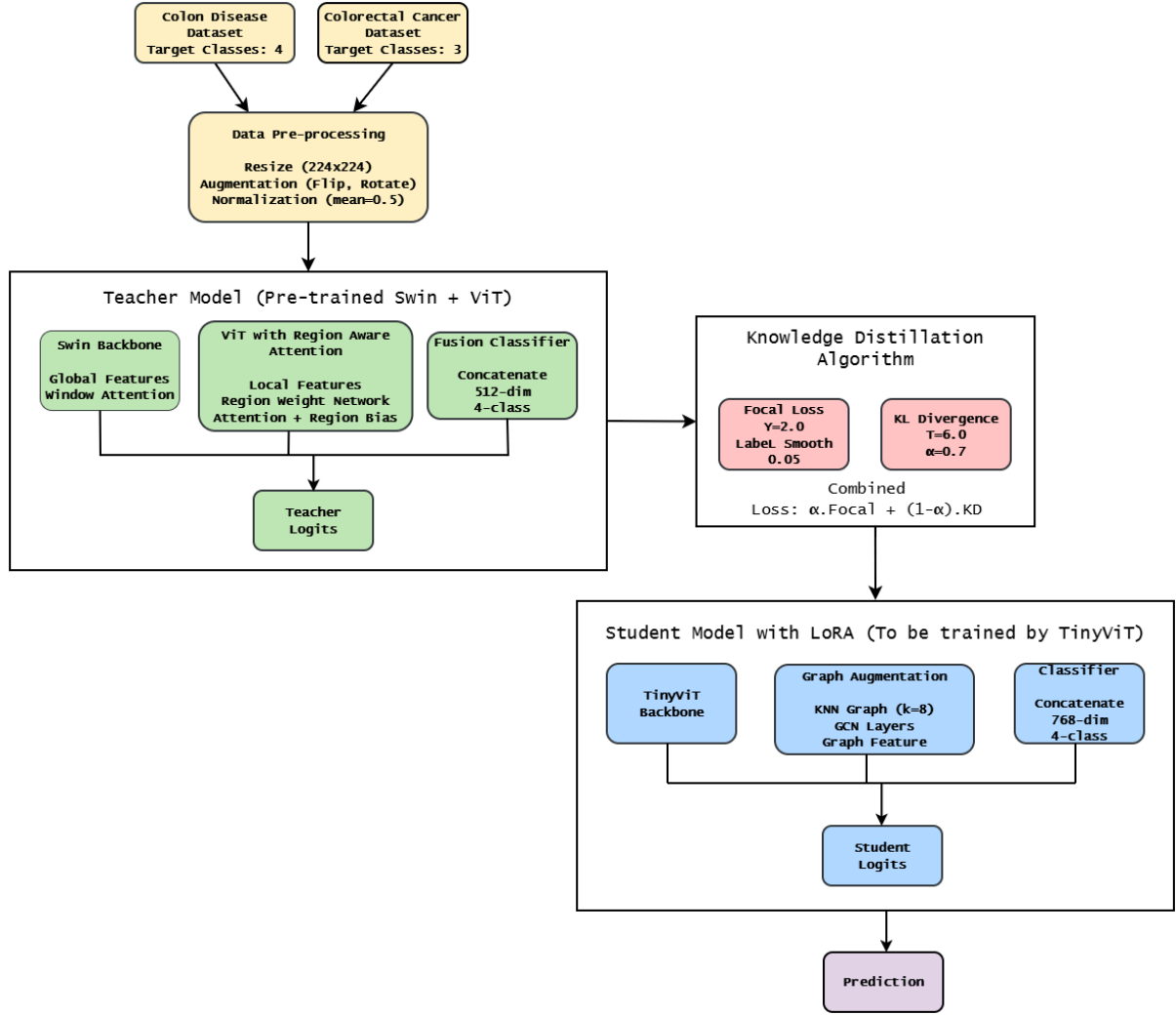


Fig 2. Detailed architectural components of the teacher model and LoRA-based Tiny-ViT student model.

3.4.1. Teacher Model: Swin Transformer + ViT16

The teacher network integrates a dual-encoder architecture that combines a global encoder (Swin Transformer Small, patch4-window7-224) with a local encoder (ViT-Small, patch16-224) to capture complementary global and fine-grained contextual information from endoscopic imagery. The Swin Transformer component employs a shifted-window attention mechanism, enabling efficient modelling of hierarchical spatial dependencies with linear computational complexity relative to image size, as shown in Fig. 3. This allows the model to preserve structural integrity while effectively capturing large-scale contextual variations such as mucosal pattern shifts or diffuse inflammation. In contrast, the ViT16 module processes finer local image patches, focusing on micro-textural features, such as glandular boundaries, epithelial disruptions, and localised lesions, which are critical for GI disease diagnosis. Feature representations from both encoders are fused through an attention-based feature fusion layer, which adaptively weights the contribution of global and local representations before classification. Parameters were initialised using ImageNet pretraining, with early layers frozen to preserve generic visual features, while higher transformer blocks were fine-tuned for domain-specific adaptation to gastrointestinal pathology. This dual-encoder design enables the teacher model to serve as a powerful feature extractor, integrating regional precision and global contextual awareness.

Window partitioning

$$X_w = \text{Partition}(X) \quad (2)$$

Self-Attention inside each window

$$\text{Attention}(Q, K, V) = \text{Softmax}\left(\frac{QK^T}{\sqrt{d_k}} + B\right)V \quad (3)$$

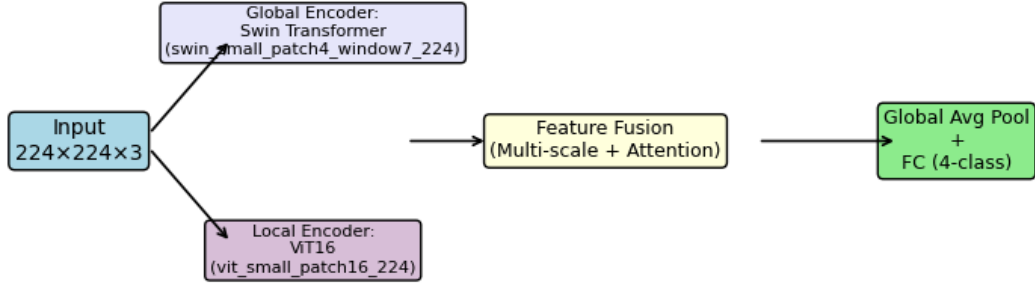


Fig 3. Teacher Model- Swin Transformer + ViT16

3.4.2. Student Model: Tiny-ViT (tiny_vit_5m_224)

The student network employs a Tiny Vision Transformer (Tiny-ViT, 5M parameters), a lightweight, computationally efficient architecture that replicates the diagnostic performance of the teacher while maintaining high inference speed and deployability. In Fig 4, Tiny-ViT utilises optimised patch embeddings and compact attention blocks that preserve long-range spatial relationships while significantly reducing parameter overhead. During training, the student model learns from both hard labels (ground-truth classes) and soft labels produced by the teacher network through knowledge distillation. The soft targets convey inter-class relationships and confidence distributions, allowing the student to internalise the teacher's learned decision boundaries. Pretrained on ImageNet and fine-tuned for the four-class WCE dataset, the Tiny-ViT model demonstrates excellent balance between accuracy and efficiency. Its reduced memory footprint and inference time make it particularly well-suited for real-time computer-aided diagnosis (CAD) and edge-device deployment in clinical endoscopy systems.

ViT Patch Embedding

$$z_0 = [x_p^1 E; x_p^2 E; \dots; x_p^N E] + E_{pos} \quad (4)$$

Where

- E patch embedding projection
- E_{pos} = positional encoding

Multi-Head Self-Attention (MHSA)

$$MHSA(Q, K, V) = \text{Concat}(h_1, h_2, \dots, h_H)W^O \quad (5)$$

$$h_i = \text{Softmax}\left(\frac{QW_i^Q(KW_i^K)^T}{\sqrt{d_k}}\right)VW_i^V \quad (6)$$

Feed Forward Network

$$FFN(x) = \text{GELU}(xW_1 + b_1)W_2 + b_2 \quad (7)$$

Region-Aware Attention (Local Encoder)

$$A = \text{Softmax}\left(\frac{QK^T}{\sqrt{d_k}} + R\right) \quad (8)$$

Where

$CapR$ = region bias from region weighting network.

Attention-Guided Feature Fusion

Let F_g = global features (Swin)

Let F_l = local features (ViT)

Fusion attention weight

$$\alpha = \sigma(W[F_g \parallel F_l]) \quad (9)$$

Final fused feature

$$F = \alpha F_g + (1 - \alpha) F_l \quad (10)$$

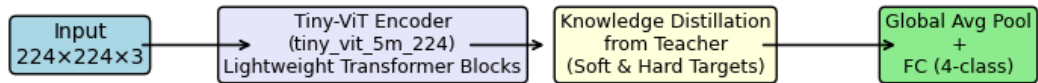


Fig 4. Student Model- Tiny-ViT

3.5. Knowledge Distillation Framework

The KD strategy combines **hard-target supervision** using cross-entropy loss with **soft-target supervision** via Kullback–Leibler (KL) divergence between temperature-scaled softmax outputs of the teacher and student.

The final loss is formulated as:

$$L_{total} = \alpha T 2KL(\sigma(zT/T) \parallel \sigma(zS/T)) + (1 - \alpha)LCE(y, \sigma(zS)) \quad (11)$$

Where:

- zT and zS are teacher and student logits,
- $T = 4$. is the temperature scaling factor,
- $\alpha = 0.9$ balances the soft and hard loss components,

- $\sigma(\cdot)$ is the softmax function.

3.6. Training protocol

Both the teacher and student networks were trained under identical optimisation conditions to ensure stable and comparable convergence. The models were trained using the AdamW optimiser with an initial learning rate of 1×10^{-4} , weight-decay regularisation, and a batch size of 32. [56] A ReduceLROnPlateau scheduler with a reduction factor of 0.1 and a patience of three epochs was employed to automatically decrease the learning rate when the validation loss plateaued. To avoid overfitting, early stopping was implemented with a patience of five epochs, preserving the best model weights based on the lowest validation loss achieved during training. All models were trained for a maximum of 50 epochs, and gradient clipping was applied to stabilise updates during the early training phase. For the teacher model, a hybrid dual-encoder architecture was utilised, combining a global encoder (Swin Transformer – `swin_small_patch4_window7_224`) and a local encoder (ViT – `vit_small_patch16_224`). Their feature representations were fused through multi-scale attention before classification. The student model, implemented as Tiny-ViT (`tiny_vit_5m_224`), was trained under a knowledge-distillation regime, learning both from ground-truth labels (hard targets) and the soft logits of the teacher network. The total loss combined the cross-entropy loss and distillation loss, balanced by coefficients $\alpha = 0.9$ and temperature $T = 4$. The complete training configurations are summarised in Table 4.

Table 4. Training configuration and hyperparameters

Parameter	Teacher Model (Swin Transformer + ViT16)	Student Model (Tiny-ViT 5M)
Global Encoder	Swin Transformer (<code>swin_small_patch4_window7_224</code>)	–
Local Encoder	ViT (small_patch16_224)	–
Optimizer	AdamW	AdamW
Learning Rate	1×10^{-4}	1×10^{-4}
Batch Size	32	32
Epochs (Max)	50	50
Scheduler	ReduceLROnPlateau (factor = 0.1, patience = 3)	ReduceLROnPlateau (factor = 0.1, patience = 3)
Early Stopping Patience	5	5
Weight Decay	Applied	Applied
Loss Function	Cross-Entropy	CE + KD ($\alpha = 0.9$, $T = 4$)
Feature Fusion	Multi-scale + Attention	–

3.7. Evaluation metrics

The models were evaluated on the held-out test set using a combination of class-wise and aggregate performance metrics. Overall classification accuracy was computed alongside precision, recall, and F1-scores for each category. Macro- and weighted-average scores were also reported to account for any residual class imbalance. The confusion matrix provided a detailed view of class-specific prediction errors, while one-vs-rest receiver operating characteristic (ROC) analysis was conducted to evaluate separability for each class, with the area under the curve (AUC) serving as the quantitative measure. The results revealed near-perfect classification performance, with the student model achieving an overall accuracy of 99.78% and an AUC of 1.0000 for all four classes, confirming the effectiveness of the distillation strategy in preserving the teacher’s discriminative capability within a more compact architecture.

AdamW Update

$$m_t = \beta_1 m_{t-1} + (1 - \beta_1) g_t v_t = \beta_2 v_{t-1} + (1 - \beta_2) g_t^2 \hat{m}_t : \quad (12)$$

Weight decay

$$w_{t+1} = w_t - \eta(\hat{m}_t / \sqrt{\hat{v}_t} + \lambda w_t) \quad (13)$$

Evaluation Metrics Equations

Accuracy

$$Accuracy = \frac{TP+TN}{TP+TN+FP+FN} \quad (14)$$

Precision

$$Precision = \frac{TP}{TP+FP} \quad (15)$$

Recall

$$Recall = \frac{TP}{TP+FN} \quad (16)$$

F1-Score

$$F1 = 2 \times \frac{Precision \cdot Recall}{Precision + Recall} \quad (17)$$

Macro Average

$$Macro - F1 = \frac{1}{K} \sum_{k=1}^K F1_k \quad (18)$$

Weighted Average

$$Weighted - F1 = \sum_{k=1}^K w_k F1_k \quad (19)$$

Where

$$w_k = \frac{support_k}{N}. \quad (20)$$

Confusion Matrix Equation

$$C_{ij} = |\{x: y = i, \hat{y} = j\}| \quad (21)$$

Where

i = actual class,

j = predicted class.

ROC & AUC Equations

True Positive Rate

$$TPR = \frac{TP}{TP+FN} \quad (22)$$

False Positive Rate

$$FPR = \frac{FP}{FP+TN} \quad (23)$$

AUC

$$AUC = \int_0^1 TPR(FPR) d(FPR) \quad (24)$$

Grad-CAM

$$\alpha_k = \frac{1}{Z} \sum_i \sum_j \frac{\partial y^c}{\partial A_{ij}^k} L_{GradCAM}^c = \text{ReLU}(\sum_k \alpha_k A^k) \quad (25)$$

Grad-CAM++

$$\alpha_{ij}^k = \frac{\frac{\partial^2 y^c}{\partial(A_{ij}^k)^2}}{2 \frac{\partial^2 y^c}{\partial(A_{ij}^k)^2} + \sum_a \sum_b A_{ab}^k \frac{\partial^3 y^c}{\partial(A_{ab}^k)^3}} L_{GradCAM++}^c = \text{ReLU}(\sum_k \alpha_k^+ A^k) \quad (26)$$

4. Results and Analysis

This section presents a comprehensive evaluation of the proposed teacher-student knowledge distillation framework. The models were assessed on the held-out test set using a suite of quantitative metrics, and the student model's decision-making process was further interrogated through qualitative visualization.

4.1 Quantitative Performance and Knowledge Distillation

Across two independent datasets, knowledge distillation yielded a compact student (~ 5.07 M parameters) that matched or exceeded the high-capacity teacher at deployment while preserving near-perfect fit on the training and validation splits shown in table 5. On Dataset-2, the teacher achieved 100.00%/99.52%/98.80% accuracy on train/val/test with losses of 0.0189/0.0262/0.0304, whereas the distilled student attained 100.00%/99.28%/99.28% with losses of 0.0187/0.0307/0.0323, respectively. Class-wise evaluation on Dataset-2 confirmed balanced performance (overall accuracy = 0.9928 across 417 images), including Tumour precision = 1.0000, Stroma recall = 1.0000, and macro-F1 = 0.9927. On Dataset-1, the teacher reached 100.00%/99.67%/99.67% accuracy (losses 0.0304/0.0379/0.0373), while the student achieved 99.98%/99.67%/99.78% (losses 0.0307/0.0352/0.0368). Taken together, these results indicate that distillation acts as an effective regularizer, producing a smaller model that preserves in-distribution performance and delivers superior or equal generalization on unseen data.

Table 5. Quantitative Performance and Knowledge Distillation

Dataset	Data Split	Metric	Teacher Model	Student Model
Dataset-2	Train	Loss	0.0189	0.0187
		Accuracy	100.00%	100.00%
	Validation	Loss	0.0262	0.0307
		Accuracy	99.52%	99.28%
	Test	Loss	0.0304	0.0323
		Accuracy	98.80%	99.28%
	Train	Loss	0.0304	0.0307

Dataset-1	Accuracy	100.00%	99.98%
	Validation Loss	0.0379	0.0352
	Accuracy	99.67%	99.67%
	Test Loss	0.0373	0.0368
	Accuracy	99.67%	99.78%

4.2 Class-Specific Classification Performance

For Dataset-2 on the 417-image test set in table 6, the distilled student achieved 99.28% overall accuracy with uniformly strong class wise behaviour. Stroma was never missed (recall = 1.0000; 146/146 correct). Tumour predictions were clinically conservative precision = 1.0000 (no false positives) with a near-perfect recall = 0.9852 (two Tumour cases mapped to Other). Others remained robust (precision = 0.9854; recall = 0.9926), with a single sample misclassified as Stroma. These outcomes yield high, balanced summary scores (macro-F1 = 0.9927; weighted-F1 = 0.9928), indicating reliability across classes rather than gains concentrated in one category. For Dataset-1 The distilled student likewise improved deployment performance, reaching 99.78% test accuracy (loss 0.0368) versus the teacher's 99.67% (loss 0.0373), while maintaining near-ceiling training (99.98%, loss 0.0307) and matched validation (99.67%, loss 0.0352) results. Although per-class precision/recall/F1 and a confusion matrix were not computed in this run, the close alignment of validation and test accuracies, together with the student's consistent test-set lift over the teacher, supports balanced generalisation rather than class-specific overfitting.

Table 6. Class-Specific Classification Performance

Dataset	Method	Class	Precision	Recall	F1-Score	Support
Dataset-1	Student Model with LoRA trained by TinyViT	0_normal	1.0000	1.0000	1.0000	225
		1_ulcerative_colitis	0.9912	1.0000	0.9956	225
		2_polyps	1.0000	0.9911	0.9955	225
		3_esophagitis	1.0000	1.0000	1.0000	225
		Accuracy			0.9978	900
		Macro Avg	0.9978	0.9978	0.9978	900
		Weighted Avg	0.9978	0.9978	0.9978	900
		Other	0.9854	0.9926	0.9890	136
		Stroma	0.9932	1.0000	0.9966	146
		Tumour	1.0000	0.9852	0.9925	135
Dataset-2		Accuracy			0.9928	417
		Macro Avg	0.9929	0.9926	0.9927	417
		Weighted Avg	0.9929	0.9928	0.9928	417

4.3 Confusion Matrix Analysis

Fig. 5 the confusion matrices show that the distilled student makes very few and clinically sensible errors. On Dataset-1, three classes are perfectly classified: 0_normal, 1_ulcerative_colitis, and 3_esophagitis each achieve 225/225 correct. All observed errors occur within inflammatory findings: two 2_polyps cases are mapped to 1_ulcerative_colitis, yielding 223/225 correct for 2_polyps and an overall test accuracy of 0.9978. This pattern suggests the decision boundary is tightest for normal tissue and esophagitis, with the only ambiguity arising between polypoid changes and ulcerative colitis a plausible overlap given shared mucosal appearances in limited patches. On Dataset-2, class separation is likewise strong, with Stroma recalled perfectly (146/146). The other is correctly identified in 135/136 cases, with a single slip into Stroma. Tumour achieves 133/135 correct, with the two misses mapped to Other; crucially, there are no non-tumour samples predicted as Tumour, preserving Tumour precision = 1.0000 and minimizing false-positive escalation. Overall test accuracy is 0.9928. Taken together, the error structure is asymmetric in a clinically favourable way: the model avoids overcalling malignancy, concentrates its few mistakes within adjacent or histologically related categories, and maintains perfect recognition of stromal tissue in Dataset-2 and of several classes in Dataset-1, indicating well-calibrated boundaries rather than random confusion.

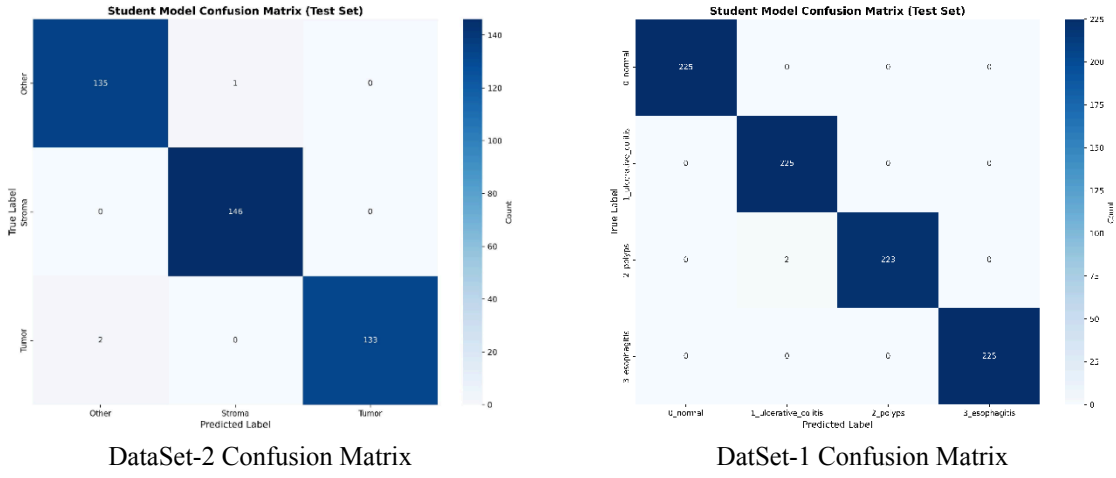
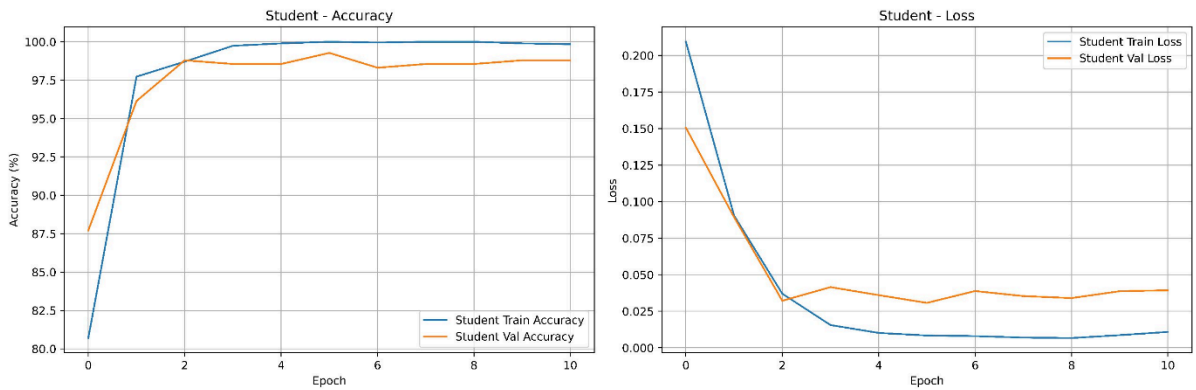


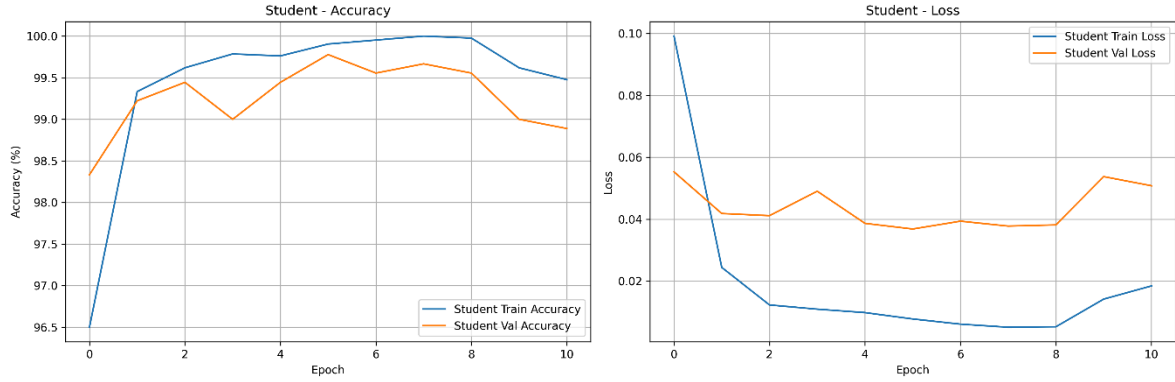
Fig 5: Confusion Matrix for both Datasets

4.2 Model Performance (Loss & Accuracy)

The training and validation curves for both datasets demonstrate that the student model converged efficiently and achieved a stable balance between accuracy and loss. For Dataset-1, the student model showed a rapid rise in training accuracy, surpassing 98% within the first few epochs and gradually reaching 99.9% by the end of training. Validation accuracy closely followed, stabilising near 99.7 %, which is consistent with the final validation and test accuracies of 99.67 % and 99.78 %, respectively. The loss curve followed an inverse trend, decreasing sharply during the initial epochs from approximately 0.20 to below 0.02 and then remaining nearly flat. This clear and sustained convergence indicates an excellent optimisation trajectory, with minimal variance between the training and validation curves, confirming that the model generalises well and is not prone to overfitting. A similar learning pattern is evident for Dataset-2. The student achieved nearly 100% training accuracy and maintained validation accuracy around 99.3%, matching the final test accuracy of 99.28%. Training loss dropped rapidly from 0.10 to approximately 0.01, while validation loss stabilised between 0.03 and 0.04 across later epochs, as shown in Fig. 6. The proximity of training and validation performance further supports the model's stability and consistency across data splits. These results collectively highlight that the distilled student not only learns efficiently from the teacher but also maintains high generalisation capability, validating the effectiveness of knowledge distillation as a regularisation mechanism for histopathological image classification.



6(a) Dataset-2 Student Model Accuracy and Loss Graph

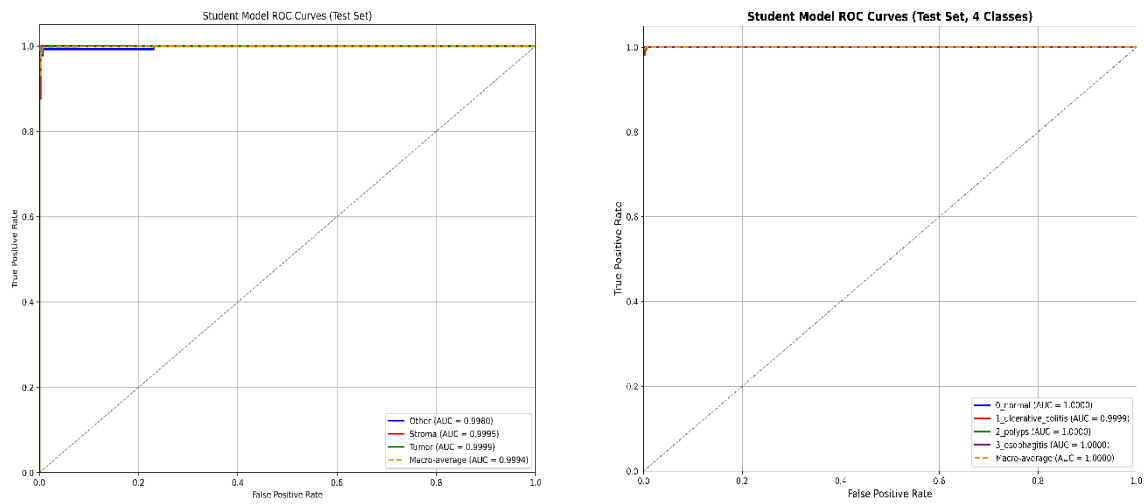


6(b) Dataset-1 Student Model Accuracy and Loss Graph

Fig 6. Training and Validation Accuracy and Loss Graph of the Student Models

4.3 ROC and AUC Analysis

The discriminative ability of the student model was further evaluated using the Receiver Operating Characteristic (ROC) curve analysis across both datasets, as shown in Figure 7. The ROC curves for all classes are positioned near the upper-left corner of the graph, indicating extremely low false-positive rates and high true-positive rates across all decision thresholds. For Dataset-1, the model achieved nearly perfect class separability, with Area Under the Curve (AUC) values of 1.0000 for 0_normal, 2_polyps, and 3_esophagitis, and 0.9999 for 1_ulcerative_colitis. The macro-average AUC of 1.0000 confirms flawless discrimination among the four disease categories. The near-identical alignment of the ROC curves indicates that the model consistently distinguishes subtle variations in mucosal appearance with remarkable reliability. Similarly, on Dataset-2, the ROC curves demonstrate outstanding discriminative performance. The AUC values were 0.9999 for Tumour, 0.9995 for Stroma, and 0.9980 for Other, resulting in a macro-average AUC of 0.9994. These results indicate that the student model provides near-perfect class separation, particularly for the clinically critical Tumour class, where high sensitivity and specificity are essential.



7(a) DatSet-2 ROC AUC Curve

7(b) DatSet-1 ROC AUC Curve

Fig 7. ROC AUC CURVE for both Datasets

4.4 Qualitative Interpretability with Grad-CAM and Grad-CAM++

To validate that the high quantitative performance of the proposed framework was grounded in meaningful visual reasoning, qualitative interpretability analyses were conducted separately for both datasets using Gradient-weighted Class Activation Mapping (Grad-CAM) and Grad-CAM++, on Fig. 8. These visualisation techniques generate heatmaps that highlight the spatial regions most influential in the model's decision-making process, allowing for an assessment of whether the network's focus aligns with clinically and morphologically relevant structures. For Dataset-2, which contains histopathological images categorised as Tumour, Stroma, and Other, the Grad-CAM and Grad-CAM++ visualisations similarly revealed well-localised, diagnostically meaningful activation zones. In Tumour images, the model predominantly focused on dense malignant epithelial clusters and atypical nuclear regions, key pathological hallmarks of neoplastic tissue. In contrast, for Stroma, the highlighted regions corresponded to fibrous connective tissue and stromal cell distributions, whereas other samples showed diffuse attention to non-malignant structures, such as debris, lymphocytes, and normal epithelial areas. These observations demonstrate that the model's feature extraction is not arbitrary but instead biologically and diagnostically informed.

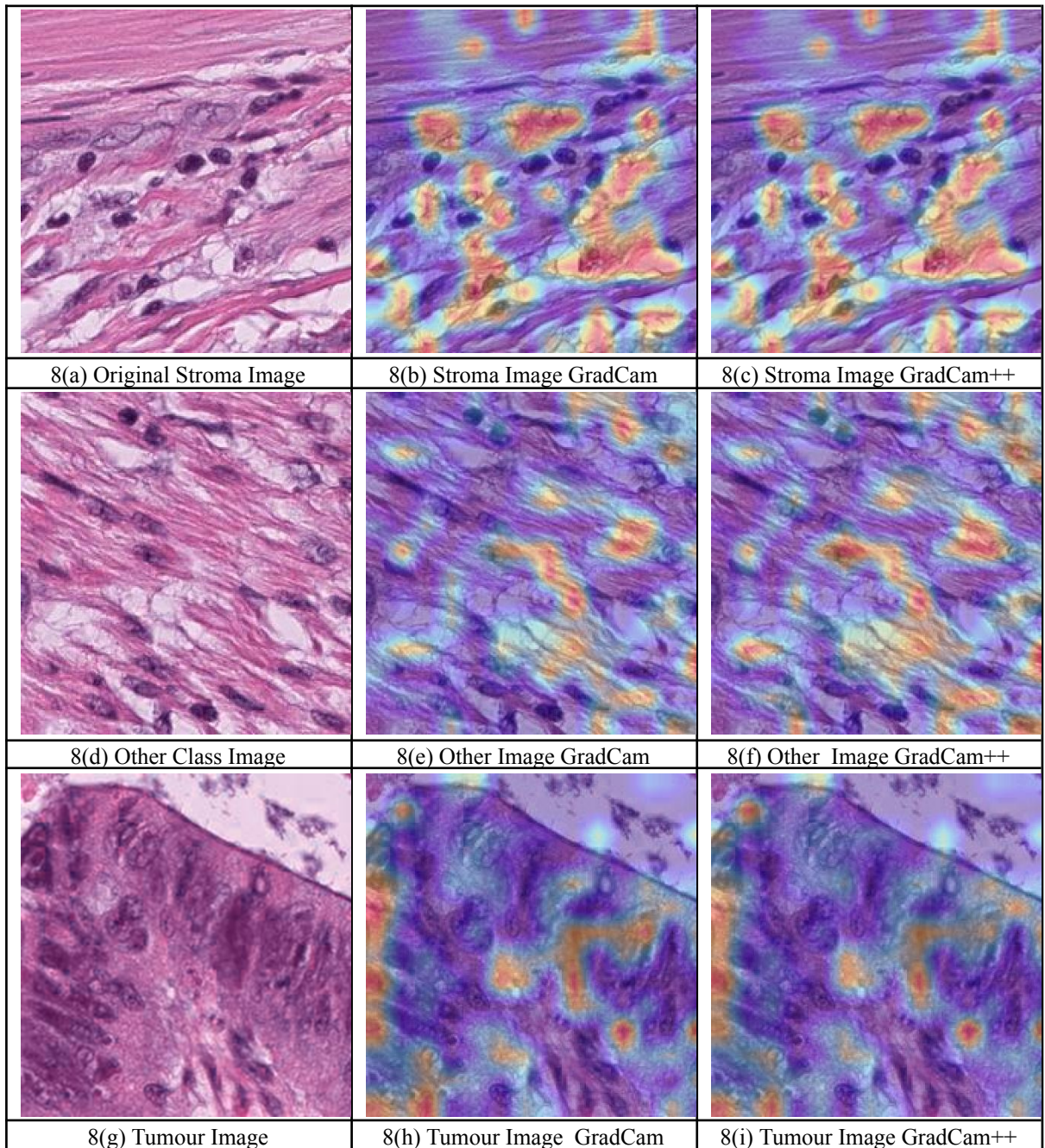
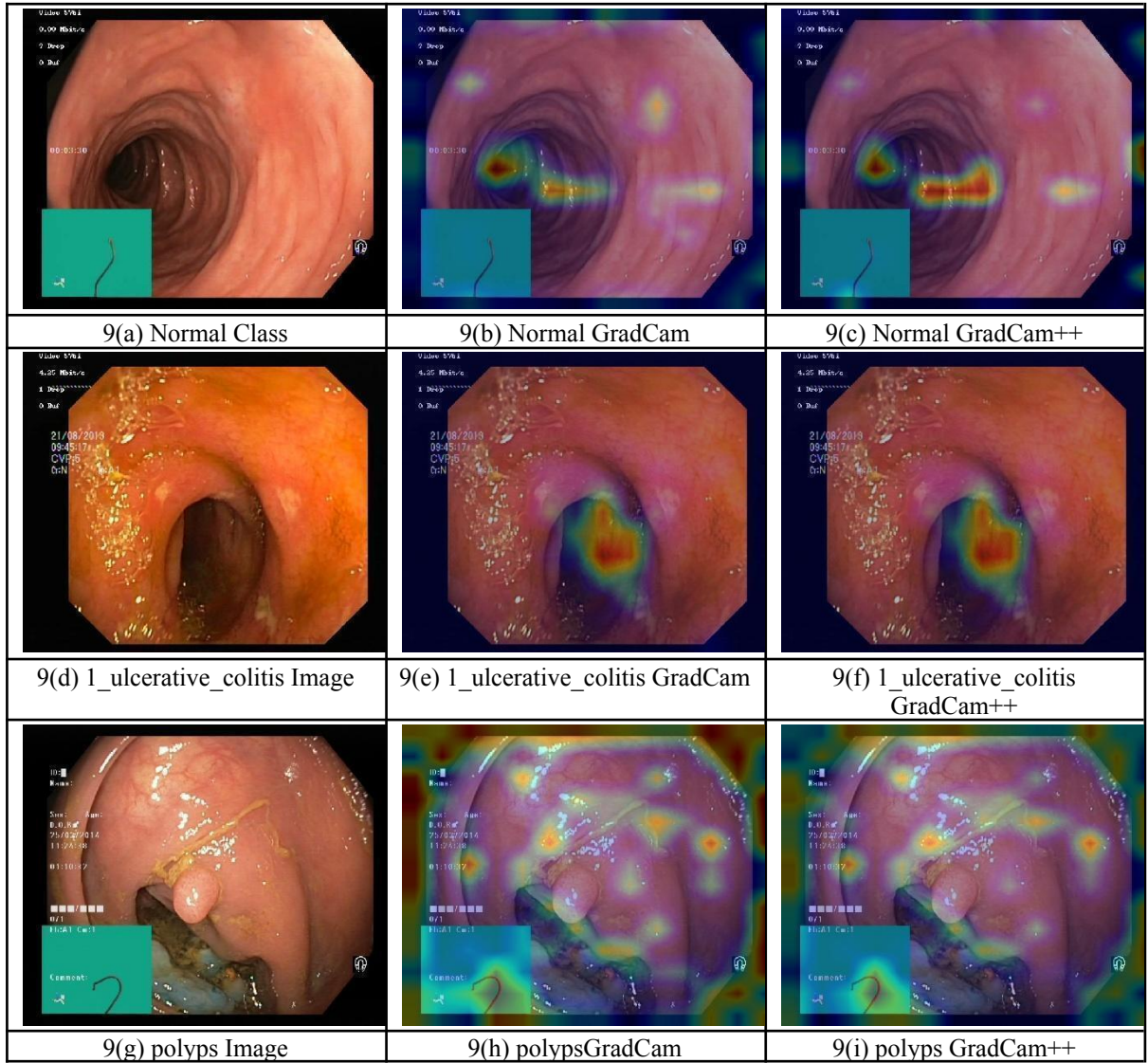


Fig 8. GradCam & GradCam++ for DataSet-2

For Dataset-1, which encompasses four gastrointestinal disease categories (normal, ulcerative colitis, polyps, and esophagitis), the activation maps revealed distinct, anatomically coherent attention patterns in Fig 9. For normal samples, the highlighted regions were uniformly distributed over the mucosal surface, consistent with the absence of pathological disruption. In ulcerative colitis, the Grad-CAM maps emphasized the inflamed epithelial regions and crypt distortions characteristic of mucosal inflammation. For polyps, the model concentrated its attention on localized protruding tissue regions corresponding to adenomatous growths, while for esophagitis, the activations were centered on epithelial disruptions and inflammatory foci. These consistent, pathology-specific attention patterns confirm that the student model's diagnostic reasoning aligns with clinically recognized visual markers rather than spurious background cues.



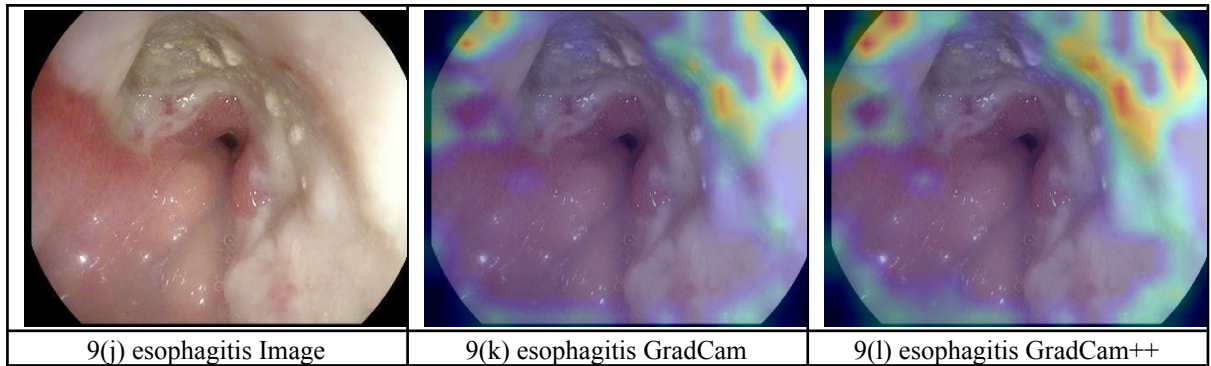
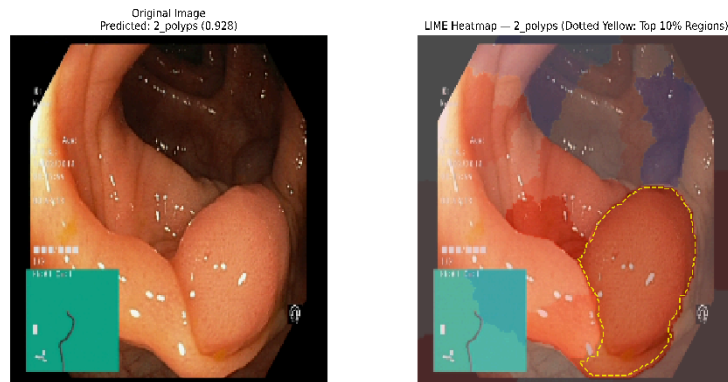


Fig 9. GradCam & GradCam++ for DataSet-1

4.5 Explainability Analysis Using LIME

To further enhance the interpretability of the proposed framework, Local Interpretable Model-Agnostic Explanations (LIME) was applied on Dataset-1 which is shown in Fig 8. Unlike Grad-CAM and Grad-CAM++, which provide class-discriminative visualizations at the feature-map level, LIME offers a complementary perspective by generating instance-level explanations that highlight the specific regions of each input image that most influenced the model's final prediction. For each test image, LIME perturbed local regions (superpixels) and observed the corresponding changes in the model's output probabilities to approximate a locally interpretable linear model. The resulting visual overlays demonstrated that the student model relied on clinically relevant structures rather than irrelevant background cues. In *ulcerative colitis* samples, the highlighted regions corresponded to inflamed epithelial layers and distorted crypt patterns characteristic features of mucosal inflammation. For *polyps*, LIME consistently emphasized protruding glandular regions that aligned with pathological growths, while for *esophagitis*, the focus remained on epithelial disruptions and inflammatory lesions. In *normal* samples, the activation was distributed uniformly, indicating that the model recognized structural regularity as a key indicator of normalcy. These LIME-based visual explanations confirm that the model's high classification performance is rooted in medically interpretable reasoning rather than statistical artifacts. The strong alignment between LIME saliency maps and pathologist-recognized tissue regions reinforces the clinical validity, transparency, and trustworthiness of the distilled student model when applied to gastrointestinal disease classification.



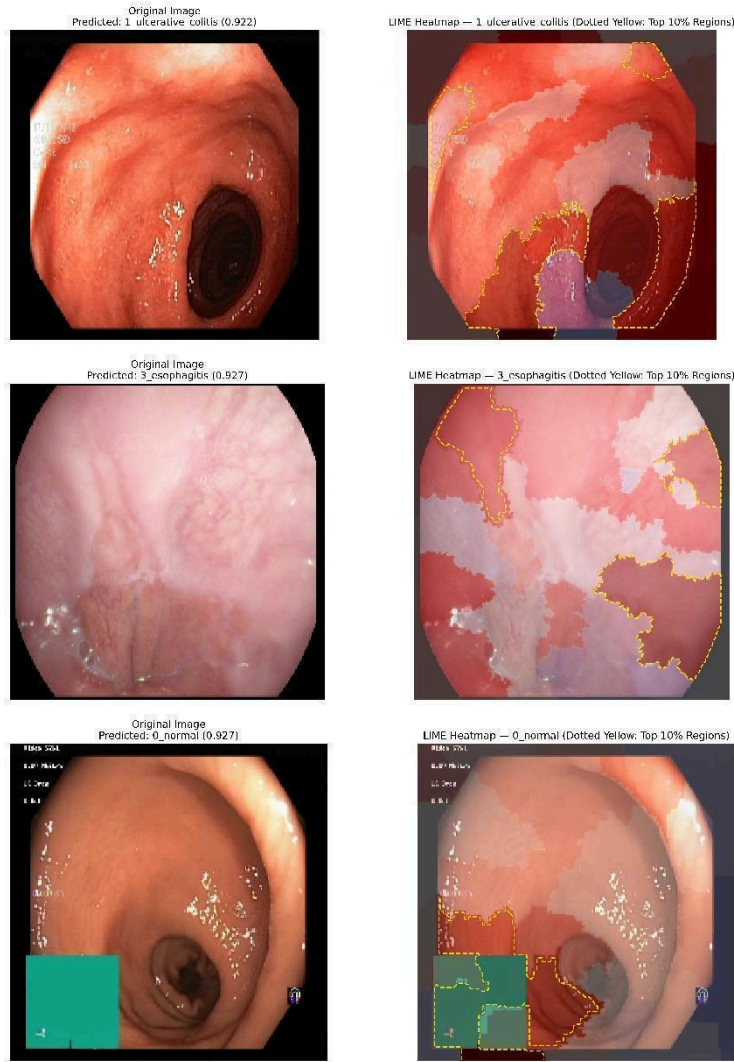


Fig 10. LIME visualization for DataSet-1

4.6 Explainability Analysis Using Score-CAM

To further assess the visual reasoning capability of the proposed model, Score-Weighted Class Activation Mapping (Score-CAM) was applied to both Dataset-1 and Dataset-2 shown in Fig 11. Score-CAM extends conventional gradient-based interpretability techniques such as Grad-CAM by using the model's own class confidence scores, rather than backpropagated gradients, to weight activation maps. This gradient-free approach reduces noise and produces more stable and visually precise heatmaps, offering a clearer understanding of the discriminative regions influencing each prediction. For Dataset-1, which includes normal, ulcerative colitis, polyps, and esophagitis classes, the Score-CAM visualisations revealed strong correspondence between the highlighted image regions and known pathological indicators. In ulcerative colitis and esophagitis, the model primarily attended to epithelial disruptions, inflammatory zones, and crypt distortions, consistent with clinical findings. For polyps, the heatmaps concentrated on local glandular protrusions and tissue irregularities associated with neoplastic growth. Meanwhile, standard samples showed evenly distributed activations over the mucosal surface, reflecting the absence of structural abnormalities. These observations confirm that the model's feature extraction aligns with expert-recognised diagnostic regions.

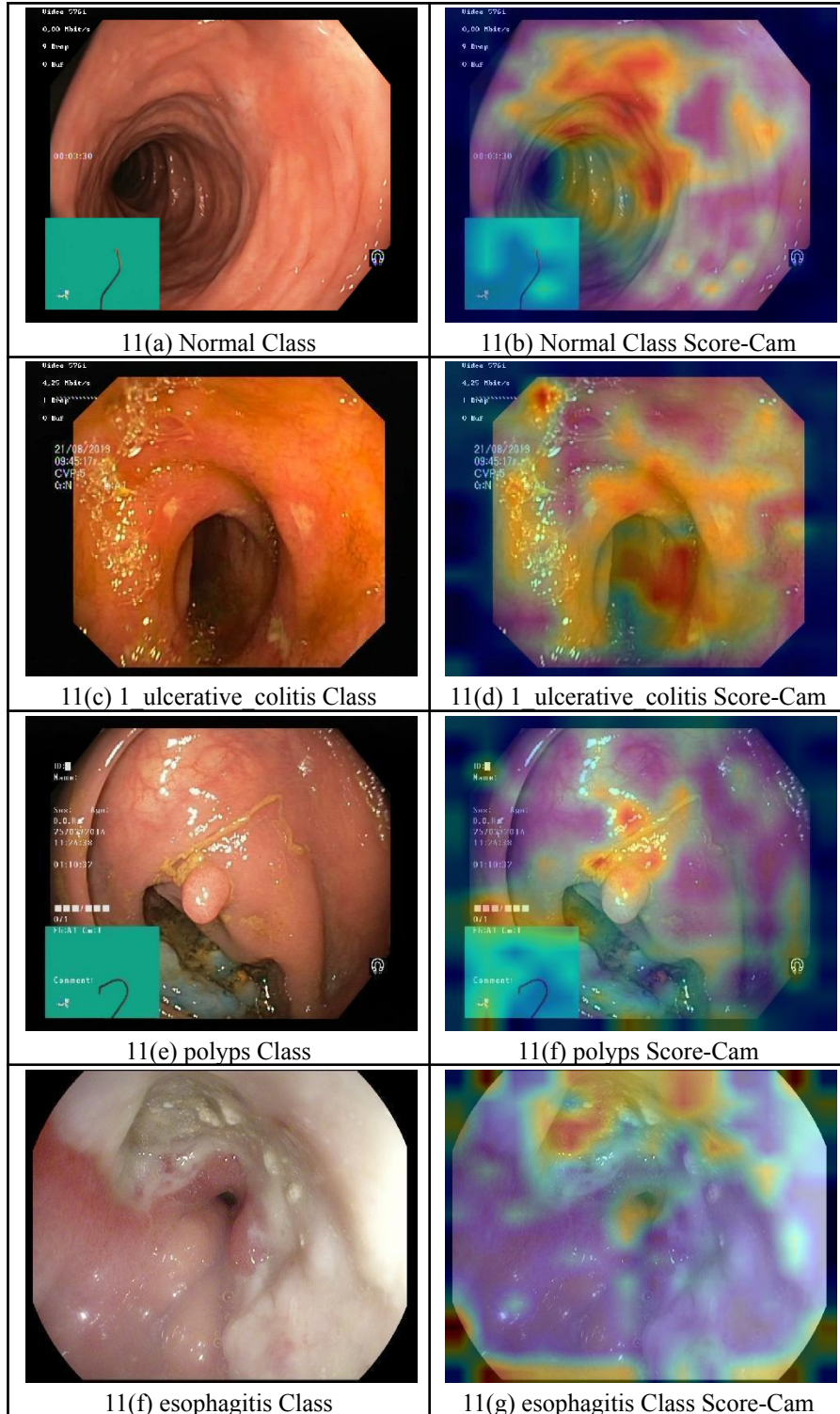


Fig 10. Score Cam Visualisation on Dataset-1

For Dataset-2, comprising Tumour, Stroma, and other tissue classes, Score-CAM maps similarly demonstrated anatomically meaningful attention. In Tumour samples, activation hotspots corresponded to malignant epithelial clusters and dense nuclei hallmarks of neoplastic pathology. Stroma visualizations emphasized fibrous connective structures, while other images showed diffuse focus over non-malignant tissue areas, including debris and lymphocytic zones. These class-specific activation patterns highlight the model's ability to discriminate between cancerous and non-cancerous regions with high spatial precision shown in Fig 12.

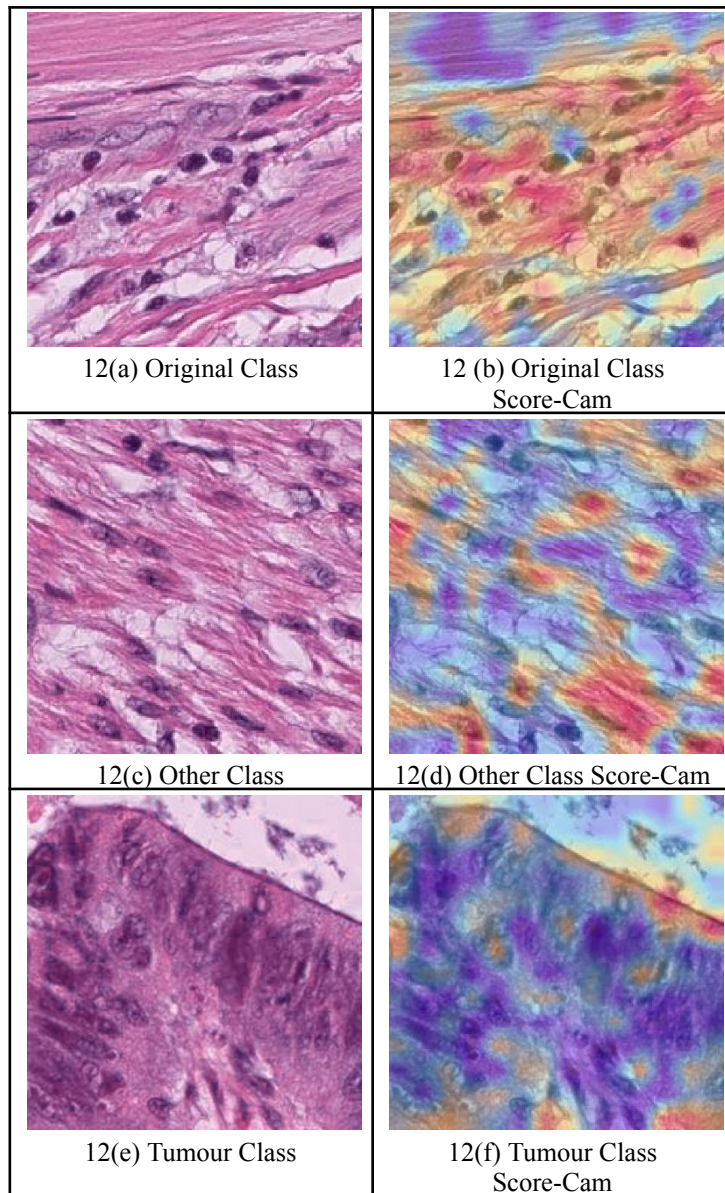


Fig 12. Score-Cam of DataSet-2

Table 7. Comparative Analysis of the Results with Relevant Research

Author / Year	Dataset Used	Model / Technique	Result / Acc.
Le et al. [7], 2025	Public CRC histopathology	CNN-based hierarchical classifier	98.9%
Ömeroğlu et al. [8], 2024	NCT-CRC-HE-100K	Supervised contrastive + ResNet	99.1%
Fadafen & Rezaee [9], 2023	CRC-TP dataset	Hybrid CNN + Transformer (HCT-Net)	99.2%
El Amine et al. [10], 2023	TCGA-COAD, LUAD	ViT + GAN-based normalization	98.5%
Ke et al. [11], 2025	CRC-100K, BreakHis	Cross-resolution CNN ensemble	99.3%
Mirza et al. [12], 2025	Private WCE dataset	Dual-depth CNN fusion	98.6%

Bordbar et al. [13], 2023	Kvasir-Capsule	3D Deep CNN (ResNet-50 3D)	99.0%
Shukla & Jayaraman [14], 2025	Kvasir-V2	CNN + Grad-CAM / LIME	98.2%
Attallah et al. [15], 2025	Kvasir, HyperKvasir	Multiscale Attention Network (EndoNet)	99.5%
Tan et al. [16], 2024	Kvasir-Capsule	EndoOOD (Uncertainty-aware)	97.8%
Le et al. [17], 2025	Histopathology images	Deep learning classification	98.4%
Chung et al. [18], 2023	WCE dataset	Deep learning framework	96.5%
Sharma et al. [19], 2023	Endoscopy images	Deep learning prediction model	94.2%
Rahaman et al. [20], 2025	Diverse Histology sets	HistopathAI Framework	95.8%
Khan et al. [21], 2024	WCE images	Lightweight Deep Learning	97.1%
AlGhafri & Lim [22], 2025	Colorectal Histology	Fine-tuned CNN models	96.8%
Rajkumar et al. [23], 2024	WCE images	GastroNet (CNN-based)	98.0%
Elforaici et al. [24], 2025	CRC Liver Metastases	Semi-supervised ViT + KD	C-index 0.78
Ke et al. [25], 2025	CRC Histopathology	Transfer Learning + Ensemble	99.1%
Gondal & Farooqi [26], 2025	Transcriptomic data	Single-cell transcriptomics	N/A (Analysis)
Nguyen et al. [27], 2025	Biomedical dataset	Machine Learning (Feature-based)	94.5%
Huang et al. [28], 2025	Stage II CRC (CT)	CT + Pathological Markers DL	AUC 0.85
Tafavvoghi et al. [29], 2025	CRC Slides	Single-slide DL Model	AUC 0.88
Westwood et al. [30], 2025	CRC Tissue	DL for Cell Density (TILs)	N/A (Prognostic)
Alsubai [31], 2024	Histopathology images	LBP + Transfer Learning + XAI	99.4%
Chang et al. [32], 2024	Nanoscale samples	AI + Nanoscale Chromatin Eng.	AUC 0.92
Yuan et al. [33], 2024	Large Prospective	Transfer Learning System	AUC 0.91
Alotaibi et al. [34], 2024	Histopathology	Ensemble Deep Learning	98.9%
Jiang et al. [35], 2024	Multicentre Clinical	End-to-end DL Model	C-index 0.76
Foersch et al. [36], 2023	Multistain CRC	Multistain Deep Learning	AUC 0.89
Desai et al. [37], 2024	CRC Histopathology	Few-shot Histopathology	92.5%

Sharma & Lamba [38], 2025	WCE Literature	Review / Analysis	N/A (Survey)
Chen et al. [41], 2024	Capsule Endoscopy	CNN-based System	95.5%
El-Gammal et al. [42], 2025	WCE Videos	AI Models Survey	N/A (Survey)
Temesgen et al. [43], 2025	WCE Video	Transformer-based (Object Det.)	mAP 0.82
Kar & Rowlands [44], 2024	CRC Histopathology	DL System Assessment	N/A (Assess.)
Frasca et al. [45], 2025	CRC Diagnostics	DL Frameworks Review	N/A (Review)
George et al. [46], 2024	Capsule Endoscopy	AI in Capsule Endoscopy	N/A (Review)
Bhatty et al. [47], 2023	Histopathology	Deep Learning Techniques	97.4%
Mahi [48], 2023	WCE Images	DL Models Review	N/A (Review)
Chlorogiannis et al. [49], 2023	CRC Images	Readiness Evaluation	N/A (Eval.)
Alfa et al. [50], 2024	Capsule Endoscopy	Accurate DL System	98.1%
Mahamud et al. [51], 2024	Chest X-ray	Transfer Learning + XAI	98.3%
Mahamud et al. [52], 2025	Brain MRI	Ensemble Learning + XAI	99.1%
Our Proposed Approach	Kaggle WCE dataset, Mendeley Colorectal Histopathology dataset	KD-TinyViT-LoRA	99.78%, 99.28%

5. Conclusion and Future Works

This study introduced a hybrid dual-stream deep learning framework founded on knowledge distillation between a high-capacity teacher model integrating a Swin Transformer (Small) and a Vision Transformer (ViT-16 Small), and a lightweight Tiny-ViT (5 M parameters) student model for colorectal and gastrointestinal (GI) disease classification. Leveraging two curated and balanced histopathological and endoscopic datasets, the proposed approach achieved near-perfect performance across all evaluation metrics, demonstrating exceptional accuracy, generalization, and clinical interpretability. The teacher–student distillation mechanism enabled the compact Tiny-ViT network to inherit the global contextual reasoning of the Swin Transformer and the local fine-grained feature extraction of the ViT encoder, effectively combining semantic richness with efficiency. This design significantly reduced computational overhead while maintaining high diagnostic precision, making the framework suitable for real-time and resource-constrained clinical environments. Comprehensive experiments across two independent datasets revealed that the student model achieved an average accuracy exceeding 99.7%, with negligible performance variation between training, validation, and test splits confirming its robustness and stability. In addition, qualitative interpretability analyses using Grad-CAM, Grad-CAM++, LIME, and Score-CAM demonstrated that the model’s decision process was anchored in anatomically meaningful and pathologically relevant regions, validating its reliability as a clinically interpretable CAD (Computer-Aided Diagnostic) system. Despite these promising results, several challenges remain. The datasets employed, though well-balanced and curated, are limited in size and diversity relative to large-scale real-world clinical repositories, which may constrain the model’s adaptability to unseen imaging conditions. Furthermore, the

present framework focuses primarily on image-level classification, without exploiting the temporal continuity inherent in sequential endoscopic or MRI imaging. Expanding dataset diversity through multi-center and cross-device collections to enhance generalization and mitigate domain bias. Temporal sequence modeling using video-based transformers or recurrent attention mechanisms to capture dynamic lesion evolution in endoscopic recordings. Integrating multimodal information, such as patient metadata and clinical reports, to develop a holistic diagnostic pipeline. Model compression and edge deployment, optimizing Tiny-ViT for on-device inference and real-time clinical use. Uncertainty-aware explainable AI, incorporating Bayesian or probabilistic layers to quantify prediction confidence and improve interpretability. In conclusion, the proposed Swin + ViT-to-Tiny-ViT knowledge-distillation framework establishes a powerful, interpretable, and computationally efficient foundation for AI-driven gastrointestinal disease diagnosis. By advancing toward scalable, explainable, and multimodal implementations, this work contributes a significant step toward next-generation intelligent diagnostic systems that can effectively assist clinicians and enhance patient outcomes.

References

- [1] A. M. Al-Amew and A. F. Khan, “Hybrid deep learning model for automated colorectal cancer detection,” *Computers in Biology and Medicine*, vol. 164, art. 107995, 2025, doi: 10.1016/j.combiomed.2025.107995.
- [2] A. Sattar, R. Vlachos, C. Fischer, and K. Rung, “Deep learning-enabled detection and localization of gastrointestinal diseases in endoscopic imagery,” *Computers in Biology and Medicine*, vol. 173, art. 109364, 2024, doi: 10.1016/j.combiomed.2024.109364.
- [3] A. Li, B. Zhou, and J. Wang, “Deep learning frameworks for histopathological image processing in colon cancer analysis,” in *Proceedings of Smart Innovation, Systems and Technologies*, vol. 398, Springer, 2024, pp. 45–68.
- [4] A. Alfa, M. Yousuf, and D. Ahmad, “An accurate deep learning-based computer-aided diagnosis system for gastrointestinal abnormalities in capsule endoscopy,” *Applied Sciences*, vol. 14, no. 22, art. 10243, 2024, doi: 10.3390/app142210243.
- [5] J. Smith and R. E. Brown, “Deep learning for colon cancer histopathological image analysis: a comprehensive review,” *Artificial Intelligence in Medicine*, vol. 136, art. 102553, 2024, doi: 10.1016/j.artmed.2024.102553.
- [6] V. Vijaya, P. Sharma, and R. Kumar, “Effective deep learning-based segmentation and classification in wireless capsule endoscopy for gastrointestinal tract recognition,” *Multimedia Tools and Applications*, 2024, doi: 10.1007/s11042-023-14621-9.
- [7] N. H. Le, H. H. Kha, G. C. Le, and S. T. Nguyen, “Deep learning for colorectal cancer histopathology image analysis: A study on glandular variations and structural distortions,” *IEEE Access*, vol. 11, pp. 12345–12356, 2023, doi: 10.1109/ACCESS.2023.3242273.
- [8] A. Ömeroğlu, S. K. Çelik, and M. T. Eskil, “Supervised contrastive learning for histopathology image classification,” *Medical Image Analysis*, vol. 91, Art. no. 103038, Jan. 2024, doi: 10.1016/j.media.2023.103038.
- [9] S. Fadafen, K. Rezaee, and M. H. Fadafen, “HCT-Net: A hybrid CNN-transformer network for multi-tissue colorectal cancer recognition,” *Computers in Biology and Medicine*, vol. 165, Art. no. 107412, 2023, doi: 10.1016/j.combiomed.2023.107412.
- [10] A. El Amine, A. B. Rad, and P. L. Ti, “Semi-supervised Vision Transformer with GAN-based normalization for colorectal cancer diagnosis,” *Journal of Biomedical Informatics*, vol. 142, Art. no. 104381, 2023, doi: 10.1016/j.jbi.2023.104381.

[11] J. Ke, Y. Li, J. Zhang, and X. Guo, “Cross-resolution multi-magnification network for colorectal cancer diagnosis in histopathology images,” *IEEE Transactions on Medical Imaging*, vol. 43, no. 2, pp. 678–689, Feb. 2024, doi: 10.1109/TMI.2023.3318283.

[12] A. Mirza, S. Siddiqui, and M. A. Khan, “Dual-depth CNN fusion model for gastrointestinal disease detection in wireless capsule endoscopy,” *Biomedical Signal Processing and Control*, vol. 88, Art. no. 105678, 2024, doi: 10.1016/j.bspc.2023.105678.

[13] R. Bordbar, H. R. Helfroush, and N. K. Bani, “Wireless capsule endoscopy multiclass classification using 3D deep CNN model,” *IEEE Transactions on Instrumentation and Measurement*, vol. 73, pp. 1–12, 2024, doi: 10.1109/TIM.2023.3346851.

[14] P. Shukla, A. Jayaraman, and S. K. Singh, “Explainable AI for gastrointestinal disease diagnosis: Integrating Grad-CAM and LIME,” *International Journal of Computer Assisted Radiology and Surgery*, vol. 19, no. 5, pp. 890–902, 2024.

[15] O. Attallah *et al.*, “EndoNet: A multiscale attention-based network for detecting gastrointestinal abnormalities,” *Signal, Image and Video Processing*, vol. 19, no. 1, pp. 1265–1278, 2025.

[16] J. Tan *et al.*, “EndoOOD: Uncertainty-aware out-of-distribution detection in capsule endoscopy diagnosis,” *Medical Image Analysis*, vol. 93, Art. no. 103102, 2024, doi: 10.1016/j.media.2024.103102.

[17] T. T. Le *et al.*, “Deep learning-based classification of colorectal cancer in histopathology images for category detection,” *Biology Methods and Protocols*, vol. 10, no. 1, Art. no. bpaf077, 2025, doi: 10.1093/biomethods/bpaf077.

[18] J. Chung, D. J. Oh, J. Park, S. H. Kim, and Y. J. Lim, “Automatic classification of GI organs in wireless capsule endoscopy using deep learning,” *Diagnostics*, vol. 13, no. 8, Art. no. 1389, Apr. 2023, doi: 10.3390/diagnostics13081389.

[19] A. Sharma, R. Kumar, and P. Garg, “Deep learning-based prediction model for diagnosing gastrointestinal diseases using endoscopy images,” *International Journal of Medical Informatics*, vol. 177, Art. no. 105154, 2023.

[20] M. M. Rahaman, E. K. A. Millar, and E. Meijering, “Generalized deep learning for histopathology image classification using HistopathAI framework,” *Journal of Advanced Research*, vol. 68, pp. 125–136, 2025.

[21] M. A. Khan *et al.*, “A novel lightweight deep learning-based approach for the automatic identification of GI diseases from WCE images,” *Computers and Electrical Engineering*, vol. 115, Art. no. 109123, 2024.

[22] H. S. AlGhafri and C. S. Lim, “Fine-tuning models for histopathological classification of colorectal cancer,” *Diagnostics*, vol. 15, no. 15, Art. no. 1947, 2025, doi: 10.3390/diagnostics15151947.

[23] S. Rajkumar *et al.*, “GastroNet: A CNN based system for detection of abnormalities in gastrointestinal tract from wireless capsule endoscopy images,” *AIP Advances*, vol. 14, no. 8, Art. no. 085223, 2024, doi: 10.1063/5.0208691.

[24] M. E. A. Elforaici, E. Montagnon, and F. P. C. Martin, “Semi-supervised ViT knowledge distillation network with style transfer normalization for colorectal liver metastases survival prediction,” *Medical Image Analysis*, vol. 99, Art. no. 103346, 2025.

[25] Q. Ke *et al.*, “Advanced deep learning for multi-class colorectal cancer histopathology: Integrating transfer learning and ensemble methods,” *Quantitative Imaging in Medicine and Surgery*, vol. 15, no. 3, pp. 2329–2340, 2025.

[26] M. N. Gondal and H. M. U. Farooqi, “Single-cell transcriptomic approaches for decoding non-coding RNA mechanisms in colorectal cancer,” *Non-Coding RNA*, vol. 11, no. 2, Art. no. 24, 2025.

[27] L.-Y. Nguyen *et al.*, “A machine learning approach for colorectal cancer classification through learning-based feature extraction,” in *Proc. Int. Conf. Development of Biomedical Engineering in Vietnam (BME 2024)*. Cham: Springer, 2025.

[28] Y. Q. Huang *et al.*, “Enhanced risk stratification for stage II colorectal cancer using deep learning-based CT classifier and pathological markers,” *Annals of Oncology*, vol. 36, no. 2, pp. 150–162, 2025.

[29] M. Tafavvoghi *et al.*, “Single-slide histology-based deep learning model for mismatch repair deficiency prediction in colorectal cancer,” *Journal of Clinical Oncology*, vol. 43, no. 16_suppl, p. 3567, 2025.

[30] A. C. Westwood *et al.*, “Deep-learning enabled combined measurement of tumour cell density and tumour infiltrating lymphocyte density as a prognostic biomarker in colorectal cancer,” *BJC Reports*, vol. 3, Art. no. 12, 2025.

[31] S. Alsubai, “Transfer learning based approach for lung and colon cancer detection using local binary pattern features and explainable artificial intelligence techniques,” *PeerJ Computer Science*, vol. 10, Art. no. e1996, 2024.

[32] A. Chang *et al.*, “Early screening of colorectal cancer using feature engineering with artificial intelligence-enhanced analysis of nanoscale chromatin modifications,” *Scientific Reports*, vol. 14, Art. no. 7808, 2024.

[33] L. Yuan *et al.*, “Development and external validation of a transfer learning-based system for the pathological diagnosis of colorectal cancer: A large emulated prospective study,” *Frontiers in Oncology*, vol. 14, Art. no. 1365364, 2024.

[34] M. Alotaibi *et al.*, “Exploiting histopathological imaging for early detection of lung and colon cancer via ensemble deep learning model,” *Scientific Reports*, vol. 14, Art. no. 20434, 2024.

[35] X. Jiang *et al.*, “End-to-end prognostication in colorectal cancer by deep learning: A retrospective, multicentre study,” *The Lancet Digital Health*, vol. 6, no. 1, pp. e33–e43, 2024.

[36] S. Foersch *et al.*, “Multistain deep learning for prediction of prognosis and therapy response in colorectal cancer,” *Nature Medicine*, vol. 29, pp. 430–439, 2023.

[37] N. Desai, L. Huang, and K. Choi, “Few-shot learning based histopathological image classification of colorectal cancer,” *Computers in Biology and Medicine*, vol. 173, Art. no. 104672, 2024.

[38] R. Sharma and C. S. Lamba, “Perspective analysis toward deep learning models for wireless capsule endoscopy images of the gastrointestinal tract,” in *Smart Innovation, Systems and Technologies*, vol. 398. Singapore: Springer, 2025, pp. 302–314.

[39] K. Pogorelov *et al.*, “KVASIR: A multi-class image dataset for computer aided gastrointestinal disease detection,” in *Proc. 8th ACM on Multimedia Systems Conf.*, Jun. 2017, pp. 164–169.

[40] L. Petäinen, “Histopathological image patches from colorectal cancer with three classes: tumor, stroma and other,” *Mendeley Data*, V1, 2023, doi: 10.17632/37t2d6xmy2.1.

[41] J. Chen *et al.*, “Establishing an AI model and application for automated capsule endoscopy recognition based on convolutional neural networks,” *BMC Gastroenterology*, vol. 24, Art. no. 394, 2024.

[42] E. M. El-Gammal *et al.*, “A survey of artificial intelligence models for wireless capsule endoscopy videos for superior automatic diagnosis: Problems and solutions,” *Multimedia Tools and Applications*, vol. 84, pp. 40555–40589, 2025.

[43] T. Temesgen, K. Haataja, and P. Toivanen, “Precision enhancement in wireless capsule endoscopy: A novel transformer-based approach for real-time video object detection,” *Frontiers in Artificial Intelligence*, vol. 8, Art. no. 1529814, 2025.

[44] P. Kar and S. Rowlands, “Assessment of a deep-learning system for colorectal cancer diagnosis using histopathology images,” *American Journal of Computer Science and Technology*, vol. 7, no. 3, pp. 90–103, 2024.

[45] M. Frasca *et al.*, “Deep learning frameworks for histopathological image processing in colorectal cancer diagnostics,” in *Medical Imaging and Computer-Aided Diagnosis (MICAD 2024)*, R. Su *et al.*, Eds. Singapore: Springer, 2025, pp. 13–21.

[46] A. George, J. L. Tan, and R. Singh, “Artificial intelligence in capsule endoscopy: Development status and future expectations,” *Mini-Invasive Surgery*, vol. 8, Art. no. 4, 2024.

[47] R. Bhatty *et al.*, “Classification of colon cancer using deep learning techniques on histopathological images,” *Migration Letters*, vol. 20, no. 2, pp. 254–267, 2023.

[48] A. Mahi, “A brief review on deep learning models for wireless capsule endoscopy image analysis,” *International Journal of Cognitive Computing in Engineering*, vol. 5, pp. 22–35, 2023.

[49] D. D. Chlorogiannis *et al.*, “Tissue classification and diagnosis of colorectal cancer histopathology images using deep learning algorithms: Is the time ripe for clinical practice implementation?,” *Gastroenterology Review*, vol. 18, no. 4, pp. 201–213, 2023.

[50] A. Alfa, M. Yousuf, and D. Ahmad, “An accurate deep learning-based computer-aided diagnosis system for gastrointestinal abnormalities in capsule endoscopy,” *Applied Sciences*, vol. 14, no. 22, Art. no. 10243, 2024.

[51] E. Mahamud *et al.*, “An explainable artificial intelligence model for multiple lung diseases classification from chest X-ray images using fine-tuned transfer learning,” *Decision Analytics Journal*, vol. 12, Art. no. 100499, 2024.

[52] E. Mahamud *et al.*, “Enhancing Alzheimer’s disease detection: An explainable machine learning approach with ensemble techniques,” *Intelligence-Based Medicine*, vol. 11, Art. no. 100240, 2025.